INORGANIC CHEMISTRY FRONTIERS

RESEARCH ARTICLE

View Article Online
View Journal

Open Access Article. Published on 28 November 2025. Downloaded on 1/23/2026 4:35:22 AM.
This article is licensed under a Creative Commons Attribution-NonCommercial 3.0 Unported Licence.

Check for updates

Cite this: DOI: 10.1039/d5qi02041g

# Catalytic activation of nitrous oxide: boryl *versus* hydride nickel complexes

Carlos J. Laglera-Gándara, Elena Mora-Fernández, Riccardo Peloso, Pablo Ríos * and Amor Rodríguez *

Received 7th October 2025,
Accepted 27th November 2025

DOI: 10.1039/d5qi02041g

rsc.li/frontiers-inorganic

The selective reduction of nitrous oxide ($N_2O$), a potent greenhouse gas with harmful effects on the ozone layer, remains a significant challenge in small-molecule activation. Herein, we report the efficient deoxygenation of $N_2O$ using bis(phosphino)boryl-nickel hydride (**3**) and bis-boryl nickel complexes (**4** and **5**) under mild conditions (1–2 bar $N_2O$, 2–5 mol% catalyst loading, and 25 °C). Both catalytic systems exhibit high activity in the presence of boranes and diboranes, achieving complete $N_2O$ conversion within 30 minutes using catecholborane as the reductant. Mechanistic investigations, including stoichiometric experiments, kinetic studies, and density functional theory (DFT) calculations support the formation of nickel boroxide intermediates, ($^{R}$PBP)Ni–$OBR_2$, as key species within the catalytic cycle, while pathways involving nickel hydroxide species, ($^{R}$PBP)Ni–OH, are disfavored. These results provide valuable mechanistic insights into key aspects of $N_2O$ reduction chemistry thereby enabling the rational design of transition-metal catalysts for the activation of small-molecules.

## Introduction

Atmospheric levels of greenhouse gases have steadily increased since preindustrial time due to human activities, with carbon dioxide, methane, and nitrous oxide being the primary contributors to the climate change.[1] According to the Intergovernmental Panel on Climate Change (IPCC), the concentrations of methane and nitrous oxide have reached unprecedented levels while current concentrations of carbon dioxide are higher than any point in history.[1,2] Commonly known as laughing gas, nitrous oxide is often associated with recreational use; however, $N_2O$ is a potent greenhouse gas, with a global warming potential 300 times greater that $CO_2$ and it is also one of the main contributors to the depletion of the ozone layer.[3] Nitrous oxide naturally occurs in the atmosphere as part of the Earth's nitrogen cycle, and has numerous natural sources. However, approximately 40% of total nitrous oxide emissions are linked to human sources including agricultural practices, fuel combustion and the industrial production of nitric and adipic acid.[4] In this context, strategies to control $N_2O$ emissions have spurred numerous investigations in recent years. $N_2O$ typically reacts as an oxidizing agent, transferring oxygen and releasing $N_2$, although, an alternative reactivity, serving as a diazo transfer reagent, has also been reported.[5,6] However, due to its inert nature, harsh reaction conditions such as elevated temperature or pressure, in the presence of heterogeneous catalysts, are usually required to achieve efficient conversion.[7] Frustrated Lewis pairs (FLPs) offer pathways for the activation of $N_2O$ under mild conditions through the formation of oxo compounds.[8] Efficient catalytic deoxygenation of $N_2O$ has been achieved using disilanes as reducing reagents in combination with catalytic amounts of fluorides or alkoxides, as demonstrated by Cantat and co-workers.[9] The Cornella group has shown that low-valent Bi(I) species can effectively reduce $N_2O$ using pinacolborane as the reducing agent.[10] Recently, Paradis and coworkers accomplished the catalytic reduction of $N_2O$ using metal-free P(III)/P(V)=O catalysis with phenyl silane as reductant.[11] In Nature, nitrous oxide is converted into dinitrogen and water by nitrous oxide reductase (NOR), which utilizes a $Cu_4S$ cluster to carry out this reaction during the denitrification process.[12] Drawing inspiration from this, many research groups have made efforts to design transition metal systems that emulate this natural process.[13–26] Their reactivity is typically associated with oxygen atom transfer reactions to form M=O bonds or metal–hydroxide, alkoxide or aryloxide species by insertion into M–H or M–C bonds, with release of $N_2$. Milstein and co-workers reported the efficient catalytic hydrogenation of $N_2O$ mediated by a Ru–H complex, where the O-insertion into the Ru–hydride bond was identified as the key step.[14,15] Similarly, the mechanism proposed by Cornella and his team for the synthesis of alcohols using $N_2O$, catalyzed by nickel, suggests an O-insertion

*Instituto de Investigaciones Químicas, Departamento de Química Inorgánica, CSIC-Universidad de Sevilla-Centro de Innovación en Química Avanzada (ORFEO-CINQA), c/Américo Vespucio 49, 41092 Sevilla, Spain.*
*E-mail: pablo.rios@iiq.csic.es, marodriguez@iiq.csic.es, carlos.laglera@iiq.csic.es, emora.fernandez@gmail.com, rpeloso@us.es*

Open Access Article. Published on 28 November 2025. Downloaded on 1/23/2026 4:35:22 AM.
This article is licensed under a Creative Commons Attribution-NonCommercial 3.0 Unported Licence.

into alkyl and aryl nickel species.[16,17] Suárez and co-workers reported the catalytic $N_2O$ reduction with pinacolborane using a CNP–Ni hydride complex, DFT analysis suggested the formation of NiOH species, resulting from the insertion of $N_2O$ into the Ni–H bond.[18–20] Lee, Baik and coworkers reported the stepwise reduction sequence from nitrate to $N_2$, using a (PNP) Ni complex.[21] Interestingly, the Mo group has presented a new perspective by proposing a cooperative iron–silicon mechanism in the deoxygenation of $N_2O$, facilitated by an iron complex containing a bis(silylene) amido ligand.[22] Recently, Chaplin and co-workers reported the catalytic reduction of $N_2O$ by insertion into a Cu–B bond, leading to the boroxide derivative, detected by $^{11}$B NMR during the catalytic reaction.[23] Encouraged by these results, we envisioned as a stimulating approach to explore the catalytic reduction of $N_2O$ by O-transfer into the Ni–H, Ni–C, and Ni–B bonds of bis(phophino)boryl nickel complexes ($^{R}$PBP)NiX (R = $^{t}$Bu, Cy; X = $CH_3$, H, Bcat (cat = catecholato), Bcat′ (cat′ = 4-methylcatecholato) (**2–5**)) developed in our group (Fig. 1).[27,28] Herein, we present a comparative analysis of the catalytic reduction of $N_2O$ using these nickel species, alongside stoichiometric reactivity studies with various boranes and diborane compounds, kinetic analyses, and DFT studies. These results provide insights into the active species involved in the reaction and propose a plausible mechanism for the activation of $N_2O$.

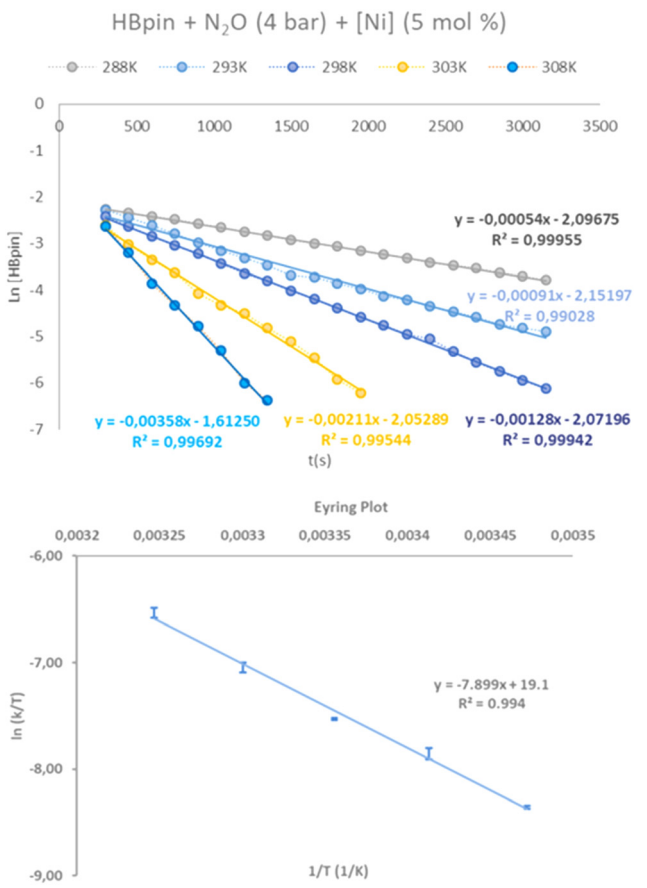


**Fig. 1** Top: Kinetic plots of ln[HBpin] *vs.* initial time (s) in $C_6D_6$ using catalyst **2a** (5 mol% catalyst loading); $P_{N_2O}$ = 4 bar; [HBpin] = 0.16 mM; $T$ = 288, 293, 298, 303 and 308 K. Bottom: Eyring plot of ln($k/T$) *vs.* 1/$T$, from 288 to 308 K, $\Delta H^{\ddagger}$ = 15.7 ± 0.7 kcal mol$^{-1}$, $\Delta S^{\ddagger}$ = −9.4 ± 0.6 cal mol$^{-1}$ K$^{-1}$, $\Delta G^{\ddagger}$ = 18.5 ± 0.9 kcal mol$^{-1}$ at 25 °C.

## Results and discussion

The synthesis of complexes ($^{tBu}$PBP)NiX (X = Br (**1a**), $CH_3$ (**2a**), H (**3**), Bcat (**4a**)) was previously reported by us[27,28] (Scheme 1). Compound ($^{Cy}$PBP)Ni$CH_3$ (**2b**) was synthesized by reaction of ($^{Cy}$PBP)NiBr (**1b**) complex with $MgMe_2$(tmeda) (tmeda = *N*,*N*,*N*′,*N*′-tetramethylethane-1,2-diamine) in pentane (see SI for details). In this reaction, $MgBr_2$(tmeda) is formed alongside **2b**, and its low solubility in pentane prevents the regeneration of **1b**, which presents a challenge for the synthesis of these species (Scheme 1).[29] Although we have previously synthesized hydride complex **3**, all attempts to prepare the hydride complex with Cy groups on phosphorus were unsuccessful. Bis-boryl nickel complexes **4b** and **5a**,**b** were prepared, using a procedure similar to that described for **4a**, by treatment of the corresponding methyl complex ($^{R}$PBP)Ni$CH_3$ (R = $^{t}$Bu (**2a**), Cy (**2b**)) with diboranes $B_2cat'_2$ and $B_2cat_2$ (Scheme 1). Compound **5a** was isolated in moderate yield, and its B{$^1$H} spectrum displayed the characteristic Ni-boryl resonances at 50 and 60 ppm. The $^{31}$P{$^1$H} NMR spectrum exhibited a signal at 117 ppm, closely matching that observed for **4a**.[28] Complexes **4b** and **5b** were fully characterized by NMR; however, all attempts to isolate them were unsuccessful due to their high sensitivity to moisture and air (see SI).

Upon treatment with $N_2O$, we observed a distinct reactivity depending on the nickel species. While the reaction of methyl complexes **2a** and **2b** with $N_2O$ did not yield any insertion product, even after heating at 70 °C for 12 hours, the nickel hydride complex $^{tBu}$PBPNiH (**3**) decomposed in the presence of $N_2O$ (see SI). In contrast, the bis(boryl) nickel derivative **4a** reacts cleanly to form the nickel boroxide complex $^{tBu}$PBPNiOBcat (**6a**) (Scheme 1; see SI for details). Complete transformation is confirmed by the disappearance of the signals corresponding to **4a** in the $^{31}$P{$^1$H} at $\delta$ 117 ppm along with the appearance of a new resonance at $\delta$ 84 ppm for the new species **6a**. The $^{11}$B{$^1$H} spectrum exhibits a resonance upfield at $\delta$ 24 ppm expected for the boroxide group. Similar reactivity was observed with analogous species **5a**, however, for complexes **4b** and **5b**, the reaction was not clean leading to the formation of several products (Scheme 1; see SI for details). To evaluate the feasibility of a hypothetical catalytic cycle, $B_2Cat_2$ was added to **6a** resulting in the recovery of bis(boryl) nickel species **4a** and the release of O(Bcat)$_2$ (Scheme 2; see SI for details). Based on these promising results, **4a** (generated *in situ* from **2a** and $B_2Cat_2$)[28] was initially selected to evaluate the catalytic reduction of $N_2O$ with $B_2Cat_2$ (Table 1).

After 19 hours at 25 °C with 5 mol% of precatalyst **2a** and 2 bar of $N_2O$, 76% conversion of $N_2O$ into $N_2$ and O(BCat)$_2$ was observed (Table 1, entry 1). Reactions carried out in toluene or fluorobenzene led to similar conversions (Table 1, entries 2

Open Access Article. Published on 28 November 2025. Downloaded on 1/23/2026 4:35:22 AM.
This article is licensed under a Creative Commons Attribution-NonCommercial 3.0 Unported Licence.

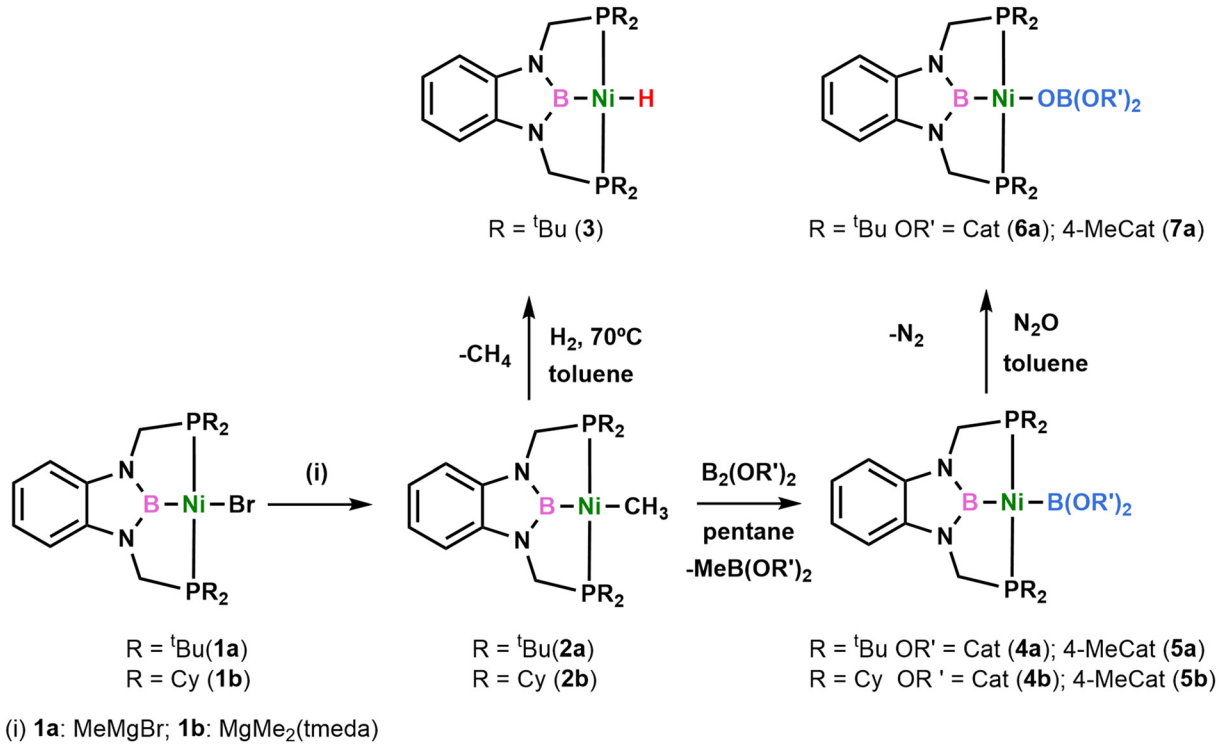


**Scheme 1** Nickel complexes tested in the reactivity with $N_2O$.

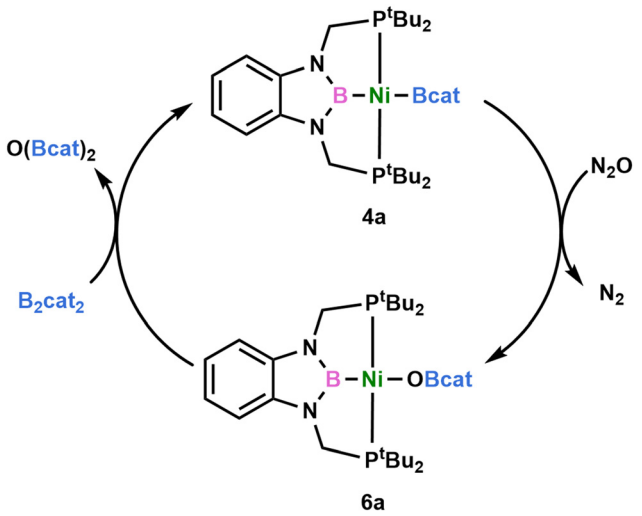


**Scheme 2** O-insertion of $N_2O$ into a Ni–B bond of **4a** and further reactivity with $B_2Cat_2$, represented as a hypothetical catalytic cycle.

and 3), while THF and $CH_2Cl_2$ showed a detrimental effect (Table 1, entries 4 and 5).[30] When the reaction was conducted at 50 °C, in $C_6D_6$, full conversion was achieved after 10 h (Table 1, entry 6). The use of a slightly more soluble diborane $B_2$(4-methylcatecholato)$_2$ ($B_2Cat_2'$) resulted in a faster reaction (Table 1, entry 7), while no reaction was observed with bis (pinacolato)diborane ($B_2pin_2$), most likely due to steric hindrance between the pinacol groups on boron and the *tert*-butyl substituents on phosphorous (Table 1, entry 8). Using complex $^{Cy}$PBPNiCH$_3$ (**2b**) as precatalyst, reduced the reaction time to just 4 hours or 3.5 h, depending on the diborane used (Table 1, entries 9 and 10). Notably, when catecholborane (HBcat) was used as the reductant, the reaction reached 99% conversion after just 30 minutes at 25 °C with **2a** as precatalyst (Table 1, entry 11). An identical conversion was also achieved within just 1 hour using only 2 mol% catalyst loading in a Fischer Porter reactor (Table 1, entry 12). Similarly, full conversion is obtained after 1.5 hours at 25 °C using pinacolborane (HBpin) (Table 1, entry 13); however, no reaction occurred with 9-BBN as reductant (Table 1, entry 14). Precatalyst **2b** proved to be less efficient with HBcat, reaching 99% conversion after 19 h (Table 1, entry 15). We tentatively attribute this low performance to the reduced stability of the nickel hydride intermediate that might be involved in this reaction (further discussion can be found below).

Notably, catalyst **3** exhibited similar conversions to **2a**, using HBcat and HBpin as reductants (Table 1, entries 16 and 17), suggesting that analogous catalytic species may be operating under these conditions. Control experiments confirmed that no reaction occurs in the absence of the nickel catalyst. These results indicate that both nickel boryl (**4a**) and hydride (**3**) complexes are highly effective catalysts for the $N_2O$ deoxygenation reaction.

To gain a deeper understanding on the nature of the nickel species involved in these catalytic reactions, individual stoichiometric reactions potentially occurring in the catalytic cycle were investigated using complexes **2–5**. As shown before, the

Open Access Article. Published on 28 November 2025. Downloaded on 1/23/2026 4:35:22 AM.
This article is licensed under a Creative Commons Attribution-NonCommercial 3.0 Unported Licence.

**Table 1** Summary of the catalytic reduction of $N_2O$ to $N_2$ [a]

| Entry | [Ni] | Solvent | $T$ | Reductant | Cat. loading mol% [b] | Time (h) | Conv. [d] (%) |
|---|---|---|---|---|---|---|---|
| 1 | **2a** | $C_6D_6$ | 25 | $B_2Cat_2$ | 5 | 19 | 76 |
| 2 | **2a** | Toluene | 25 | $B_2Cat_2$ | 5 | 19 | 75 |
| 3 | **2a** | $C_6H_5F$ | 25 | $B_2Cat_2$ | 5 | 19 | 75 |
| 4 | **2a** | THF | 25 | $B_2Cat_2$ | 5 | 10 | — |
| 5 | **2a** | $CH_2Cl_2$ | 25 | $B_2Cat_2$ | 5 | 10 | — |
| 6 | **2a** | $C_6D_6$ | 50 | $B_2Cat_2$ | 5 | 10 | 99 |
| 7 | **2a** | $C_6D_6$ | 50 | $B_2Cat'_2$ | 5 | 6 | 99 |
| 8 | **2a** | $C_6D_6$ | 50 | $B_2pin_2$ | 5 | 10 | 0 |
| 9 | **2b** | $C_6D_6$ | 50 | $B_2Cat_2$ | 5 | 4 | 99 |
| 10 | **2b** | $C_6D_6$ | 50 | $B_2Cat'_2$ | 5 | 3.5 | 99 |
| 11 | **2a** | $C_6D_6$ | 25 | HBcat | 5 | 0.5 | 99 |
| 12[c] | **2a** | $C_6D_6$ | 25 | HBcat | 2 | 1 | 99 |
| 13 | **2a** | $C_6D_6$ | 25 | HBpin | 5 | 2 | 99 |
| 14 | **2a** | $C_6D_6$ | 25 | 9-BBN | 5 | 2 | 0 |
| 15 | **2b** | $C_6D_6$ | 25 | HBcat | 5 | 19 | 99 |
| 16 | **3** | $C_6D_6$ | 25 | HBcat | 5 | 0.5 | 99 |
| 17 | **3** | $C_6D_6$ | 25 | HBpin | 5 | 1.5 | 99 |

[a] Reaction conditions, unless otherwise specified: 2 bar $N_2O$, $C_6D_6$ (400μL), [HBcat] 0.2 mM; [HBpin] 0.2 mM; [$B_2Cat_2$] = 0.2 mM. [b] The catalyst loading is calculated based on the amount of catalyst related to the amount of reductant used. [c] Reaction carried out in a Fisher Porter reactor; $P_{N_2O}$ = 1 bar. [d] Conversion was determined by $^{11}B\{^1H\}$ NMR spectroscopy using $BH_3(NMe_3)$ as an internal standard. The formation of $N_2$ and $H_2$ was detected by GC-MS analysis of the headspace gas and $^1H$ NMR spectroscopy, respectively (see SI).

reaction of **6a** with $B_2Cat_2$ results in the formation of **4a** accompanied by the generation of $O(Bcat)_2$ (Scheme 3). A similar reactivity is observed when HBcat is used; however, in this case, the nickel hydride derivative **3** is formed (Scheme 3).

Treatment of **3** with $N_2O$ results in a mixture of unidentified products (pathway *a* in Scheme 4, see SI). The formation of the product from $N_2O$ insertion into the Ni–H bond was not observed, even when the reaction was monitored by $^1H$ and $^{31}P$ NMR spectroscopy at variable temperature (from −60 °C to 25 °C). In contrast, when **3** reacts with $N_2O$ in the presence of HBcat, the reaction cleanly produces complex **6a**, along with release of $H_2$ and $N_2$ (pathway *b* in Scheme 4). We hypothesized that the reaction begins with the formation of complex $^{t\mathrm{Bu}}$PBPNi$H_2$Bcat (**8**) from nickel hydride **3** and HBcat (pathway *c* in Scheme 4), which then reacts with $N_2O$ to ultimately produce **6a**, accompanied by the elimination of $H_2$ and $N_2$ (pathway *d* in Scheme 4). To prove our hypothesis, **8** was prepared, by reacting **3** with HBcat (or alternatively by reaction of **4a** with $H_2$),[22] then, $N_2O$ was added. The generation of **6a** and release of $H_2$ was confirmed by $^1H$, $^{31}P\{^1H\}$ and $^{11}B\{^1H\}$ NMR spectroscopy (see SI).[31] Based on these experimental results we propose that nickel boroxide complex **6a** may serve as a key intermediate in the catalytic reaction and, the potential pathway involving the initial generation of nickel hydroxide species can be ruled out.

Following a detailed analysis of each step in the catalytic reaction, we carried out kinetic studies to assess the dependence of the reaction rate on each component involved. The experiment was performed using precatalyst **2a**, 2 bar of $N_2O$ and HBpin (0.08 mmol) in $C_6D_6$. The time-dependence of the conversion of HBpin into $O(Bpin)_2$ was monitored by $^{11}B\{^1H\}$ NMR spectroscopy. Initial experiments revealed that the reaction is first-order in HBpin and zero order with respect to $N_2O$. Kinetic studies varying the concentration of **2a** showed a first-order dependence on the catalyst consisting with an overall rate law of $k_{obs}$[**2a**][HBpin] (see SI for details). To estimate experimentally the thermodynamic parameters of the overall energy barrier, ($\Delta H^{\ddagger}$, $\Delta S^{\ddagger}$, and $\Delta G^{\ddagger}$), the reaction was monitored at various temperatures ranging from 15 to 35 °C (Fig. 1).

An Eyring analysis, based on a plot of $\ln(k/T)$ *versus* $1/T$, yielded an activation enthalpy ($\Delta H^{\ddagger}$) of 15.7 ± 0.7 kcal mol$^{-1}$ and activation entropy ($\Delta S^{\ddagger}$) of −9.4 ± 0.6 cal mol$^{-1}$ K$^{-1}$. The corresponding Gibbs free energy of activation ($\Delta G^{\ddagger}$) at 298 K was calculated to be 18.5 ± 0.9 kcal mol$^{-1}$.

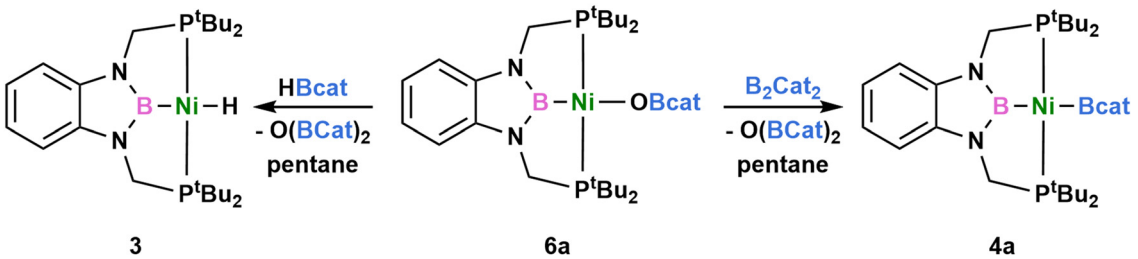


**Scheme 3** Reactivity of *t*BuPBPNiOBcat (**6a**) with $B_2Cat_2$ to form **4a** (right) and with HBcat to form **3** (left).

Open Access Article. Published on 28 November 2025. Downloaded on 1/23/2026 4:35:22 AM.
This article is licensed under a Creative Commons Attribution-NonCommercial 3.0 Unported Licence.

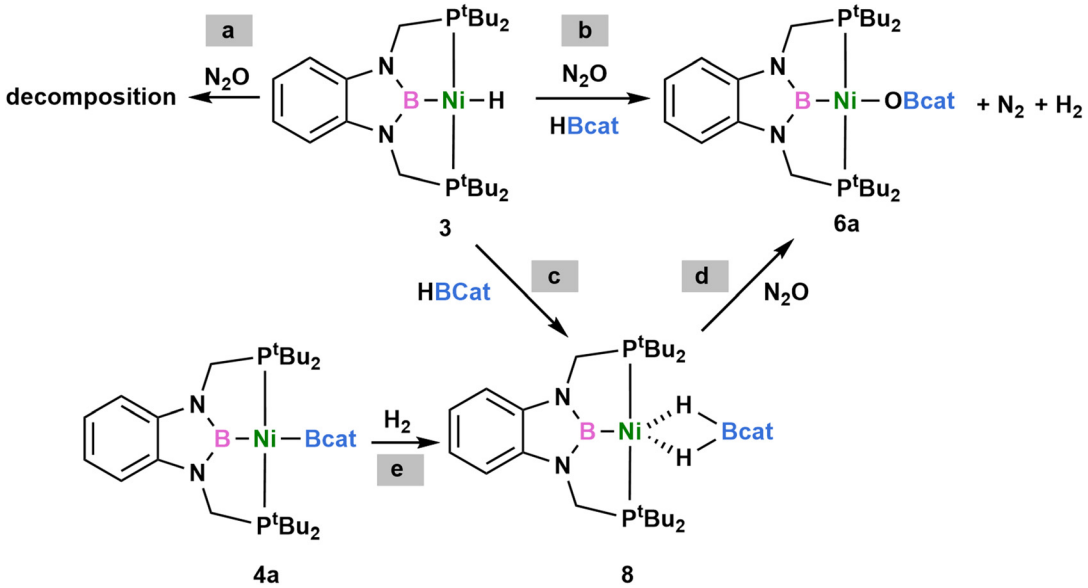


**Scheme 4** Reactivity studies of **3** with $N_2O$ and HBcat.

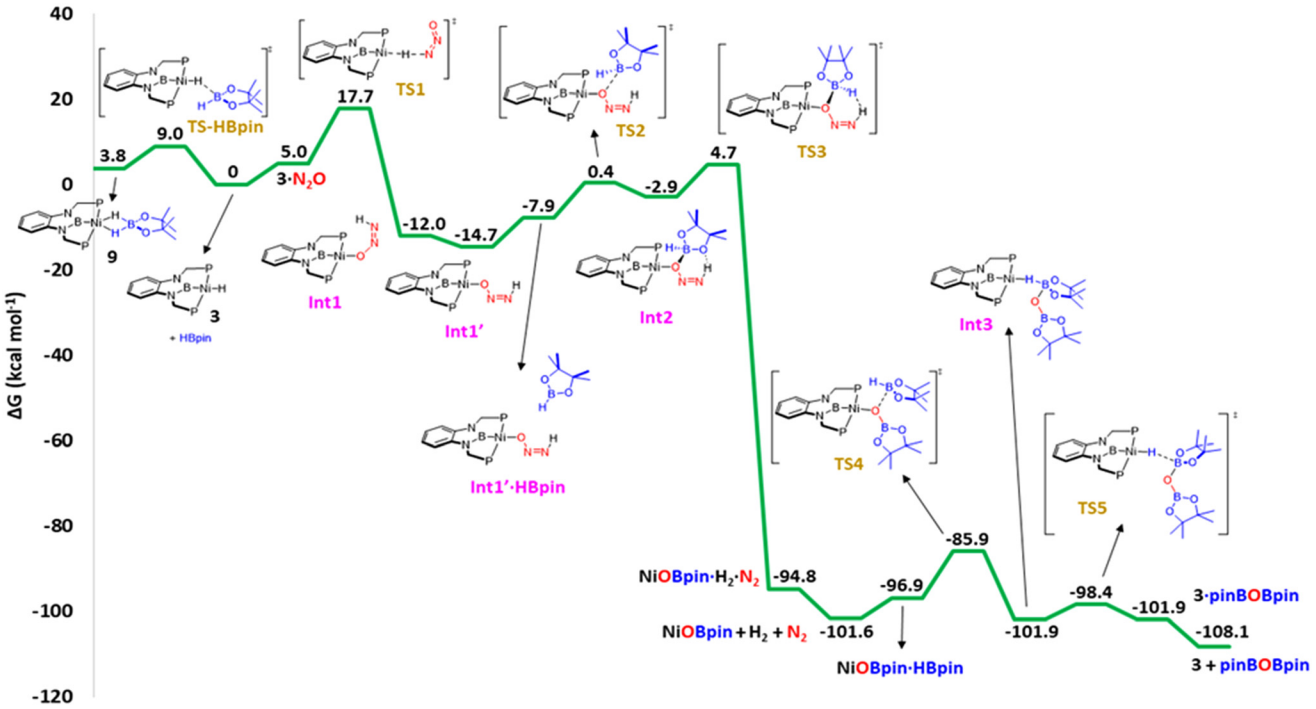


**Fig. 2** Computed Gibbs energy profile in benzene (SMD) for the reduction of $N_2O$ mediated by complex **3** and HBpin. Relative Gibbs energies computed at 298 K and 1 M are given in kcal mol$^{-1}$. The Gibbs energy of **3** + $N_2O$ + HBpin (2 equiv.) has been taken as zero energy. All data have been computed at the SMD-PBE0-D3/def2-TZVP/def2-QZVP&SDD//SMD-PBE0-D3/6-31G(d,p)&SDD(+f) level.

The reduction of $N_2O$ mediated by PBP-supported Ni complexes was also explored using DFT methods. Initial investigations involved the reaction between hydride species **3** and $N_2O$, where nucleophilic attack of the hydride moiety to the terminal nitrogen on $N_2O$ starts the catalytic transformation.[32] This step requires 17.7 kcal mol$^{-1}$ (**TS1**, Fig. 2), which is a considerably lower value than that calculated for recent examples involving picoline-derived CNP ligands,[18] probably due to the increased hydride character of **3** as a consequence of the strong *trans* influence boryl fragment.[29,33] Following the hydride transfer, intermediates **Int1** and **Int1′** (−12.0 and −14.7 kcal mol$^{-1}$, respectively) were found in the potential

Open Access Article. Published on 28 November 2025. Downloaded on 1/23/2026 4:35:22 AM.
This article is licensed under a Creative Commons Attribution-NonCommercial 3.0 Unported Licence.

energy surface, and represent a formal insertion of $N_2O$ into the Ni–H bond. From these complexes, attempts to extrude $N_2$ with concomitant formation of a hypothetical and experimentally unobserved Ni hydroxo species were pursued by a number of methods. Some of these include intramolecular 4-membered transition states (similar to what was previously found for related species),[18] participation of the PBP ligand, hydride transfer to the central nitrogen atom on $N_2O$, or processes containing two $N_2O$ molecules (more details can be found in the SI). However, all these pathways led to very high energy kinetic barriers (≥30 kcal mol$^{-1}$), in line with the experimental observations and the lack of a stable isolable or detectable Ni–OH complex. Therefore, the inclusion of a hydroborane to continue with the $N_2O$ reduction process is necessary, as experimentally found. HBpin was considered for these calculations, in order to compare the calculated energy barrier with that derived from the kinetic experiments. Similar to that described above for $N_2O$, the hydride ligand on **3** can attack the Lewis acidic boron atom of HBpin *via* **TS-HBpin** (9.0 kcal mol$^{-1}$), but the resulting hydridoborate **9** is unstable towards dissociation (3.8 kcal mol$^{-1}$), leaving HBpin available in the reaction mixture (nonetheless, $N_2O$ activation mediated by **9** has also been computationally explored, see SI for more information). Thus, the oxygen atom in intermediate **Int1′** can attack HBpin *via* **TS2**, 0.4 kcal mol$^{-1}$ above the energy reference. The result of this interaction is the corresponding adduct **Int2** (−2.9 kcal mol$^{-1}$), where the HBpin molecule and the O–N═N–H moiety establish a 6-membered ring stabilized by an O···H hydrogen bond (1.87 Å). Rotation of the HBpin molecule places the hydridic H atom close to the proton of the O–N═N–H group, which leads to the formation of dihydrogen with concomitant liberation of $N_2$ *via* **TS3**. This transition state is the rate-determining step in the proposed mechanism with an energy barrier of 19.4 kcal mol$^{-1}$, in very good agreement with that obtained experimentally (18.5 ± 0.9 kcal mol$^{-1}$). The preorganization imposed by the hydrogen bond in **Int2** leads to a rigid transition state where the orientation of the HBpin and ONNH fragments are key for the formation of the $H_2$ molecule. Expectedly, the entropy for the rate-determining step of this mechanism is negative (−3.9 cal mol$^{-1}$ K$^{-1}$), in accordance with the experimental value (−9.4 ± 0.6 cal mol$^{-1}$ K$^{-1}$). The formation of thermodynamically stable by-products translates into an abrupt decrease in energy after liberation of $N_2$ and $H_2$, placing boroxide complex NiOBpin 101.6 kcal mol$^{-1}$ below the energy reference. Regeneration of catalytically active species **3** derives from the approach of another equivalent of HBpin. In a similar manner to what was described for **TS2**, the oxygen atom in NiOBpin can attack the boron atom of HBpin *via* **TS4** (−85.9 kcal mol$^{-1}$). The participation of two Bpin fragments and the associative character of this transition state involves a negative entropic term (−22.9 cal mol$^{-1}$ K$^{-1}$). However, instead of obtaining the expected adduct where oxygen remains bound to the metal center, a subtle shift takes place to yield **Int3**, which can be described as a σ-borane complex, with Ni–H and B–H bond distances of 1.65 and 1.35 Å, respectively. From this geometry, decoordination of the bis(boryl)ether only requires 3.5 kcal mol$^{-1}$ through **TS5**, which gives back hydride species **3**.

## Conclusion

In summary, we have synthetized a number of nickel methyl, hydride and boryl complexes supported by diphosphino boryl ligands to test their reactivity with nitrous oxide. We have demonstrated that R–PBP–nickel boryl (**4–5**) and hydride (**3**) complexes are active catalysts for the deoxygenation of $N_2O$ with release of $N_2$, using boranes and diboranes as reductants, under mild conditions. Stoichiometric experiments revealed that oxygen transfer from $N_2O$ to the Ni–B bond affords novel nickel boroxide species, PBPNi–$OBR_2$ (**6–7**), whereas reaction with the nickel hydride derivative leads to unidentified decomposition products. Furthermore, our investigations establish that in both cases nickel boroxides serve as key intermediates within the catalytic cycle, thereby excluding the participation of nickel hydroxide species when nickel hydride species **3** is used. Detailed kinetic analyses combined with DFT calculations indicate that the catalytic cycle is initiated by the insertion of $N_2O$ into the nickel–hydride bond, generating a Ni–ONNH intermediate. Rather than forming nickel–hydroxide species and liberating $N_2$, this intermediate reacts directly with HBcat, releasing $N_2$ and $H_2$, and generating Ni–OBcat, which serves as the catalytically active species. Overall, this work provides a deeper understanding of $N_2O$ deoxygenation pathways and offer valuable information for the design of versatile platforms for small molecules activation reactions.

## Methods

### General procedure for the catalytic reduction of $N_2O$ with RPBPNiX species 2a (R = $^t$Bu; X = $CH_3$), 2b (R = Cy; X = $CH_3$) and 3 (R = $^t$Bu; X = H)

To a high-pressure J. Young valve NMR tube containing the catalyst or precatalyst (5 or 2 mol%), $C_6D_6$ (500 μL) and borane or diborane (0.08 mmol) were added and the J. Young valve NMR tube was degassed *via* three freeze–pump–thaw cycles. Then, the J. Young valve NMR tube was backfilled with $N_2O$ gas (2 bar). The reaction mixture was placed in a water bath at 25 °C and monitored by $^{11}B\{^1H\}$ NMR spectroscopy using $BH_3(NMe_3)$ as an internal standard. All reactions were performed in duplicate in deuterated solvent.

### Computational details

Calculations were performed using the PBE0 functional,[34] as implemented in Gaussian 09[35] along with Grimme's D3 dispersion correction.[36] Geometry optimizations were performed in solution (solvent = benzene, $\varepsilon$ = 2.27) using the continuum SMD model[37] and basis set 1 (BS1). BS1 uses the double-ζ 6-31G(d,p)[38] basis set for the H, C, N, O, B, and P atoms and the scalar relativistic Stuttgart–Dresden SDD pseudopotential[39] and its associated double-ζ basis set, complemented with a set

Open Access Article. Published on 28 November 2025. Downloaded on 1/23/2026 4:35:22 AM. This article is licensed under a Creative Commons Attribution-NonCommercial 3.0 Unported Licence.

of polarization functions, for the Ni atom.[40] The nature of the stationary points was confirmed by frequency analysis. Connections between the transition states and the minima were checked by perturbing the transition state geometry along the TS coordinate and optimizing until the corresponding minima. All energies in solution were corrected by single-point calculations with the larger basis set 2 (BS2) including triple-ζ def2TZVP basis set for the H, C, N, O, B, and P atoms, and def2QZVP for the Ni atom.[41] The scalar relativistic Stuttgart–Dresden SDD pseudopotential and its associated basis set for Ni was used in the energy profile calculations. Gibbs energies in benzene were calculated at 298.15 K. Gibbs energy corrections were obtained based on vibrational frequencies of the BS1 optimized structures using the quasi-harmonic approximation. Thermal contributions to the Gibbs energies were corrected by employing the approximation described by Grimme, where entropic terms for frequencies below a cut-off of 100 $cm^{-1}$ were calculated using the free-rotor approximation.[42] The GoodVibes program developed by Paton and Funes-Ardoiz was employed to introduce these corrections.[43] All reported energies in the main text correspond to PBE0-D3/BS2 Gibbs energies in benzene solvent (1 M) at 298.15 K in kcal $mol^{-1}$. Structure visualization was performed with Chemcraft software.[44]

## Author contributions

C. J. L. G., E. M. F. and A. R. performed the experimental work. R. P. performed the analysis of the kinetic data. P. R. performed the DFT calculations. R. P., P. R. and A. R. wrote the manuscript. A. R. conceived the project and directed the work. All authors have given approval to the final version of the manuscript.

## Conflicts of interest

There are no conflicts to declare.

## Data availability

The data supporting this article have been included as part of the supplementary information (SI). Supplementary information: synthesis and characterization details; experimental procedures, kinetic studies, compound characterization data, NMR spectra (PDF) and extended computational details (PDF). Cartesian coordinates and energies of optimized structures (XYZ). See DOI: **https://doi.org/10.1039/d5qi02041g**.

## Acknowledgements

This work was supported by the Spanish MCIN/AEI/10.13039/501100011033 (PID2022-141925NB-I00 and RED2022-134287-T). C. J. Laglera-Gándara thanks for a Margarita Salas grant financed by the European Union-Next Generation EU, Ministry of Universities and Recovery, Transformation and Resilience Plan, through a call from University of Oviedo (Grant MU-21-UP2021-030 53307942). The use of the computational facilities of the Supercomputing Center of Galicia (CESGA) is gratefully acknowledged.

## References

1 IPCC, in *Climate Change 2023: Synthesis Report. Contribution of Working Groups I, II and III to the Sixth Assessment Report of the Intergovernmental Panel on Climate Change*, ed. Core Writing Team, H. Lee and J. Romero, IPCC, Geneva, Switzerland, 2023, 184 pp., DOI: DOI: **10.59327/IPCC/AR6-9789291691647**.
2 J. Hansen and M. Sato, Greenhouse Gas Growth Rates, *Proc. Natl. Acad. Sci. U. S. A.*, 2004, **101**, 16109–16114.
3 A. R. Ravishankara, J. S. Daniel and R. W. Portmann, Nitrous Oxide ($N_2O$): The Dominant Ozone-Depleting Substance Emitted in the 21st Century, *Science*, 2009, **326**, 123–125.
4 H. Tian, R. Xu, J. G. Canadell, R. L. Thompson, W. Winiwarter, P. Suntharalingam, E. A. Davidson, P. Ciais, R. B. Jackson, G. Janssens-Maenhout, *et al.*, A Comprehensive Quantification of Global Nitrous Oxide Sources and Sinks, *Nature*, 2020, **586**, 248–256.
5 K. Severin, Synthetic Chemistry with Nitrous Oxide, *Chem. Soc. Rev.*, 2015, **44**, 6375–6386.
6 A. Genoux and K. Severin, Nitrous Oxide as Diazo Transfer Reagent, *Chem. Sci.*, 2024, **15**, 13605–13617.
7 V. N. Parmon, G. I. Panov and A. S. Noskov, Nitrous Oxide in Oxidation Chemistry and Catalysis: Application and Production, *Catal. Today*, 2005, **100**, 115–131. A number of metal (Cu, Ru, ...) surfaces catalyze this transformation at cryogenic temperatures and (sub)ambient pressures. See: W. A. Brown, R. K. Sharma, D. A. King and S. Haq, Adsorption and Reactivity of NO and $N_2O$ on Cu{110}: Combined RAIRS and Molecular Beam Studies, *J. Phys. Chem.*, 1996, **100**, 12559–12568.
8 D. W. Stephan and G. Erker, Frustrated Lewis Pair Chemistry of Carbon, Nitrogen and Sulfur Oxides, *Chem. Sci.*, 2014, **5**, 2625–2641.
9 L. Anthore-Dalion, E. Nicolas and T. Cantat, Catalytic Metal-Free Deoxygenation of Nitrous Oxide with Disilanes, *ACS Catal.*, 2019, **9**, 11563–11567.
10 Y. Pang, M. Leutzsch, N. Nöthling and J. Cornella, Catalytic Activation of $N_2O$ at a Low-Valent Bismuth Redox Platform, *J. Am. Chem. Soc.*, 2020, **142**, 19473–19479.
11 R. Zhou, V. Medvarić, T. Werner and J. Paradies, Metal-Free Reduction of Nitrous Oxide via PIII/PV═O Cycling: Mechanistic Insights and Catalytic Performance, *J. Am. Chem. Soc.*, 2025, **147**, 37879–37884.
12 A. Pomowski, W. Zumft, P. M. H. Kroneck and O. Einsle, $N_2O$ Binding at a [4Cu:2S] Copper–Sulphur Cluster in Nitrous Oxide Reductase, *Nature*, 2011, **477**, 234–237.

Open Access Article. Published on 28 November 2025. Downloaded on 1/23/2026 4:35:22 AM.
This article is licensed under a Creative Commons Attribution-NonCommercial 3.0 Unported Licence.

13 W. B. Tolman, Binding and Activation of $N_2O$ at Transition-Metal Centers: Recent Mechanistic Insights, *Angew. Chem., Int. Ed.*, 2010, **49**, 1018–1024.
14 R. Zeng, M. Feller, Y. Ben-David and D. Milstein, Hydrogenation and Hydrosilylation of Nitrous Oxide Homogeneously Catalyzed by a Metal Complex, *J. Am. Chem. Soc.*, 2017, **139**, 5720–5723.
15 R. Zeng, M. Feller, Y. Diskin-Posner, L. J. W. Shimon, Y. Ben-David and D. Milstein, CO Oxidation by $N_2O$ Homogeneously Catalyzed by Ruthenium Hydride Pincer Complexes Indicating a New Mechanism, *J. Am. Chem. Soc.*, 2018, **140**, 7061–7064.
16 F. Le Vaillant, A. Mateos Calbet, S. Rodriguez-Pelayo, E. J. Reijerse, S. Ni, J. Busch and J. Cornella, Catalytic Synthesis of Phenols with Nitrous Oxide, *Nature*, 2022, **604**, 677–683.
17 S. Ni, F. Le Vaillant, A. Mateos-Calbet, R. Martin and J. Cornella, Ni-Catalyzed Oxygen Transfer from $N_2O$ onto $sp^3$-Hybridized Carbons, *J. Am. Chem. Soc.*, 2022, **144**, 18223–18228.
18 J. Bermejo, I. Ortega-Lepe, L. L. Santos, N. Rendón, J. López-Serrano, E. Álvarez and A. Suárez, Nitrous Oxide Activation by Picoline-Derived Ni–CNP Hydrides, *Chem. Commun.*, 2024, **60**, 1575–1578.
19 I. Ortega-Lepe, P. Sánchez, L. L. Santos, P. Lara, N. Rendón, J. López-Serrano, V. Salazar-Pereda, E. Álvarez, M. Paneque and A. Suárez, Catalytic Nitrous Oxide Reduction with $H_2$ Mediated by Pincer Ir Complexes, *Inorg. Chem.*, 2022, **61**, 18590–18600.
20 J. Bermejo, L. L. Santos, E. Álvarez, J. López-Serrano and A. Suárez, Oxidation of Alcohols to Carboxylates with $N_2O$ Catalyzed by Ruthenium(II)-CNC Complexes, *ACS Catal.*, 2025, **15**, 11530–11543.
21 J. Gwak, S. Ahn, M.-H. Baik and Y. Lee, One Metal is Enough: A Nickel Complex Reduces Nitrate Anions to Nitrogen Gas, *Chem. Sci.*, 2019, **10**, 4767.
22 X. Chen, H. Wang, S. Du, M. Driess and Z. Mo, Deoxygenation of Nitrous Oxide and Nitro Compounds Using Bis(N-Heterocyclic Silylene)Amido Iron Complexes as Catalysts, *Angew. Chem., Int. Ed.*, 2022, **61**, e202114598.
23 T. M. Hood, R. S. C. Charman, D. J. Liptrot and A. B. Chaplin, Copper(I) Catalysed Diboron(4) Reduction of Nitrous Oxide, *Angew. Chem., Int. Ed.*, 2024, e202411692.
24 J. S. Stanley, X. S. Wang and J. Y. Yang, Selective Electrocatalytic Reduction of Nitrous Oxide to Dinitrogen with an Iron Porphyrin Complex, *ACS Catal.*, 2023, **13**, 12617–12622.
25 J. L. Martinez, J. E. Schneider, S. W. Anferov and J. S. Anderson, Electrochemical Reduction of $N_2O$ with a Molecular Copper Catalyst, *ACS Catal.*, 2023, **13**, 12673–12680.
26 A. W. Beamer and J. A. Buss, Surface-like $NO_x$ Reduction at an Atomically-Precise Tricopper Cluster, *Angew. Chem., Int. Ed.*, 2025, **64**, e202424772.
27 N. Curado, C. Maya, J. López-Serrano and A. Rodríguez, Boryl-Assisted Hydrogenolysis of a Nickel–Methyl Bond, *Chem. Commun.*, 2014, **50**, 15718–15721.
28 P. Ríos, J. Borge, F. Fernández de Córdoba, G. Sciortino, A. Lledós and A. Rodríguez, Ambiphilic Boryl Groups in a Neutral Ni(II) Complex: A New Activation Mode of $H_2$, *Chem. Sci.*, 2021, **12**, 2540–2548.
29 A. P. Deziel, M. R. Espinosa, L. Pavlovic, D. J. Charboneau, N. Hazari, K. H. Hopmann and B. Q. Mercado, Ligand and Solvent Effects on $CO_2$ Insertion into Group 10 Metal Alkyl Bonds, *Chem. Sci.*, 2022, **13**, 2391–2404.
30 We believe that the low catalytic activity observed when using THF and $CH_2Cl_2$ is related to the limited stability of the catalyst in both solvents. In $CH_2Cl_2$, nickel hydride or nickel boryl species are likely converted into nickel chloride species, which are catalytically inactive. In the case of THF, we attribute the low stability of the catalyst to the presence of traces amount of water in the solvent.
31 We have carried out the reaction of nickel hydride **3** with 10 equiv. of HBpin (Fig. S29 and 30 in the SI). In the $^{31}P\{^1H\}$ NMR no significant changes were observed; however, in the $^1H$ NMR spectra the hydride resonance of **3** (−1.7 ppm, triplet, $J_{P-H}$ = 34.8 Hz) disappeared upon mixing **3** with HBpin. These observations suggest that **3** and HBpin might reversibly form an adduct in which a hydride bridges both Ni and B atoms, with the equilibrium shifted toward the left side, favoring the formation of **3**. Additionally, when this mixture is exposed to $N_2O$, the formation of $O(Bpin)_2$ is observed with generation of $H_2$.
32 The activation of $N_2O$ mediated by boryl complex **4a** was also pursued, but very high energy barriers (≥32 kcal $mol^{-1}$) were obtained in all cases. See SI for more details.
33 P. Ríos, A. Rodríguez and J. López-Serrano, Mechanistic Studies on the Selective Reduction of $CO_2$ to the Aldehyde Level by a Bis(phosphino)boryl (PBP)-Supported Nickel Complex, *ACS Catal.*, 2016, **6**, 5715.
34 C. Adamo and V. Barone, Toward Reliable Density Functional Methods without Adjustable Parameters: The PBE0 Model, *J. Chem. Phys.*, 1999, **110**, 6158–6170.
35 M. J. Frisch, G. W. Trucks, H. B. Schlegel, G. E. Scuseria, M. A. Robb, J. R. Cheeseman, G. Scalmani, V. Barone, B. Mennucci, G. A. Petersson, H. Nakatsuji, M. Caricato, X. Li, H. P. Hratchian, A. F. Izmaylov, J. Bloino, G. Zheng, J. L. Sonnenberg, M. Hada, M. Ehara, K. Toyota, R. Fukuda, J. Hasegawa, M. Ishida, T. Nakajima, Y. Honda, O. Kitao, H. Nakai, T. Vreven, J. A. Montgomery Jr., J. E. Peralta, F. Ogliaro, M. Bearpark, J. J. Heyd, E. Brothers, K. N. Kudin, V. N. Staroverov, T. Keith, R. Kobayashi, J. Normand, K. Raghavachari, A. Rendell, J. C. Burant, S. S. Iyengar, J. Tomasi, M. Cossi, N. Rega, J. M. Millam, M. Klene, J. E. Knox, J. B. Cross, V. Bakken, C. Adamo, J. Jaramillo, R. Gomperts, R. E. Stratmann, O. Yazyev, A. J. Austin, R. Cammi, C. Pomelli, J. W. Ochterski, R. L. Martin, K. Morokuma, V. G. Zakrzewski, G. A. Voth, P. Salvador, J. J. Dannenberg, S. Dapprich, A. D. Daniels, O. Farkas, J. B. Foresman, J. V. Ortiz, J. Cioslowski and D. J. Fox, *Gaussian 09, Revision E.01*, Gaussian, Inc., Wallingford, CT, 2013.

Open Access Article. Published on 28 November 2025. Downloaded on 1/23/2026 4:35:22 AM.
This article is licensed under a Creative Commons Attribution-NonCommercial 3.0 Unported Licence.

36 S. Grimme, J. Antony, S. Ehrlich and H. Krieg, A Consistent and Accurate Ab Initio Parametrization of Density Functional Dispersion Correction (DFT-D) for the 94 Elements H–Pu, *J. Chem. Phys.*, 2010, **132**, 154104.

37 A. V. Marenich, C. J. Cramer and D. G. Truhlar, Universal Solvation Model Based on Solute Electron Density and a Continuum Model of the Solvent, *J. Phys. Chem. B*, 2009, **113**, 6378–6396.

38 (*a*) W. J. Hehre, R. Ditchfield and J. A. Pople, Self–Consistent Molecular Orbital Methods. XII. Further Extensions of Gaussian–Type Basis Sets for Use in Molecular Orbital Studies of Organic Molecules, *J. Chem. Phys.*, 1972, **56**, 2257–2261; (*b*) P. C. Hariharan and J. A. Pople, The Influence of Polarization Functions on Molecular Orbital Hydrogenation Energies, *Theor. Chim. Acta*, 1973, **28**, 213–222; (*c*) M. M. Francl, W. J. Pietro, W. J. Hehre, J. S. Binkley, M. S. Gordon, D. J. DeFrees and J. A. Pople, Self–Consistent Molecular Orbital Methods. XXIII. A Polarization–Type Basis Set for Second–Row Elements, *J. Chem. Phys.*, 1982, **77**, 3654–3665.

39 M. Dolg, U. Wedig, H. Stoll and H. Preuss, Energy–Adjusted Ab Initio Pseudopotentials for the Rare Earth Elements, *J. Chem. Phys.*, 1987, **86**, 866–872.

40 A. W. Ehlers, M. Boehme, S. Dapprich, A. Gobbi, A. Höllwarth, V. Jonas, K. F. Köhler, R. Stegmann, A. Veldkamp and G. Frenking, A Set of f–Polarization Functions for Pseudo–Potential Basis Sets of the Transition Metals Sc–Cu, Y–Ag, and La–Au, *Chem. Phys. Lett.*, 1993, **208**, 111–114.

41 (*a*) F. Weigend and R. Ahlrichs, Balanced Basis Sets of Split Valence, Triple Zeta Valence and Quadruple Zeta Valence Quality for H to Rn: Design and Assessment of Accuracy, *Phys. Chem. Chem. Phys.*, 2005, **7**, 3297–3305; (*b*) F. Weigend, Accurate Coulomb-Fitting Basis Sets for H to Rn, *Phys. Chem. Chem. Phys.*, 2006, **8**, 1057–1065.

42 S. Grimme, Supramolecular Binding Thermodynamics by Dispersion-Corrected Density Functional Theory, *Chem. – Eur. J.*, 2012, **18**, 9955–9964.

43 G. Luchini, J. V. Alegre-Requena, I. Funes-Ardoiz and R. S. Paton, GoodVibes: Automated Thermochemistry for Heterogeneous Computational Chemistry Data, *F1000Research*, 2020, **9**, 291.

44 Chemcraft – Graphical Software for Visualization of Quantum Chemistry Computations. Available online: **https://www.chemcraftprog.com**.